Isoreticular Tolerance and Phase Selection in the Synthesis of Multi-Module Metal-Organic Frameworks for Gas Separation and Electrocatalytic OER

Yuchen Xiao,[a] Xianhui Bu,*[b] and Pingyun Feng*[a]

[a] Dr. Y. Xiao, Prof. P. Feng
Department of Chemistry
University of California, Riverside
900 University Ave, Riverside, CA 92521 (USA)
E-mail: pingyun.feng@ucr.edu

[b] Prof. X. Bu
Department of Chemistry and Biochemistry
California State University Long Beach
1250 Bellflower Boulevard, Long Beach, CA 90840 (USA)
E-mail: xianhui.bu@csulb.edu

Supporting information for this article is given via a link at the end of the document.

Abstract: Although metal-organic frameworks are coordination-driven assemblies, the structural prediction and design using metal-ligand interactions can be unreliable due to other competing interactions. Leveraging non-coordination interactions to develop porous assemblies could enable new materials and applications. Here, we use a multi-module MOF system to explore important and pervasive impact of ligand-ligand interactions on metal-ligand as well as ligand-ligand co-assembly process. It is found that ligand-ligand interactions play critical roles on the scope or breakdown of isoreticular chemistry. With cooperative di- and tri-topic ligands, a family of Ni-MOFs has been synthesized in various structure types including partitioned MIL-88-acs (*pacs*), interrupted *pacs* (i-*pacs*), and UMCM-1-muo. A new type of isoreticular chemistry on the muo platform is established between two drastically different chemical systems. The gas sorption and electrocatalytic studies were performed that reveal excellent performance such as high C_2H_2/CO_2 selectivity of 21.8 and high C_2H_2 uptake capacity of 114.5 cm^3/g at 298 K and 1 bar.

The success or failure in the structural prediction and design of new materials is closely correlated to the understanding of fundamental interactions between molecular building blocks. Because metal-organic frameworks (MOFs) are coordination assemblies, the factors that impact coordination interactions and geometry, such as the nuclearity and geometry of clusters, the type and geometry of ligand functional groups, are usually relied upon to predict and design new MOF materials.[1] This is the basis for isoreticular chemistry which refers to the efforts to change structural components and tune pore properties while retaining the underlying framework topology.[2] In the context of isoreticular chemistry, a concept called isoreticular tolerance can be useful. The isoreticular tolerance can be understood as the capacity of a MOF platform to retain its structure type upon component substitutions. A tolerant MOF platform means topological insensitivity towards component changes. This can result from the situations where the co-assemblies between framework components are dictated by metal-ligand coordination interactions and as a result the change at the core or on the backbone of ligands wouldn't generate interactions disruptive enough to change the framework topology.

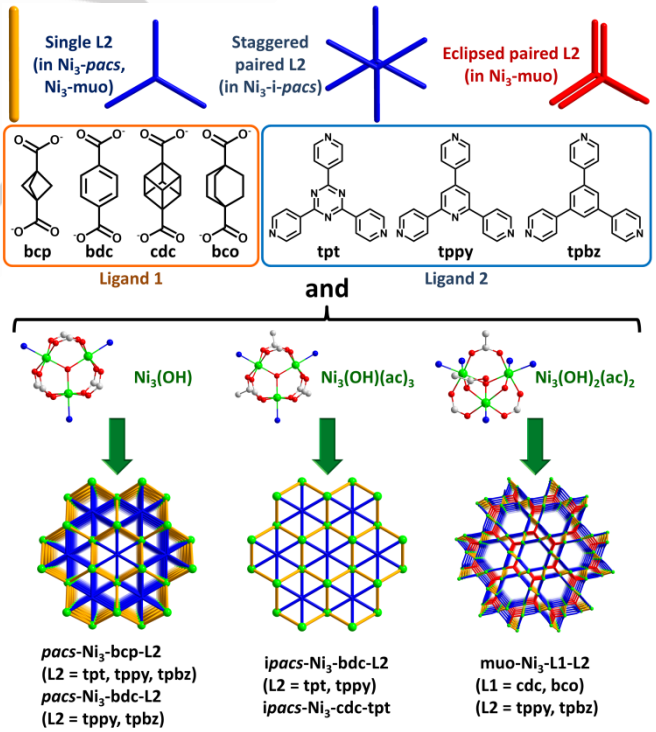

Figure 1. Illustration of three multi-module MOF types in this work. bcp = bicyclo[1.1.1]pentane-1,3-dicarboxylate, bdc = benzene-1,4-dicarboxylate, cdc=1,4-cubanedicarboxylate, bco=bicyclo[2.2.2]octane-1,4-dicarboxylate, tpt=2,4,6-tri(4-pyridyl)-1,3,5-triazine, tppy=2,4,6-tris(4-pyridyl)pyridine, and tpbz=1,3,5-tri(4-pyridyl)benzene.

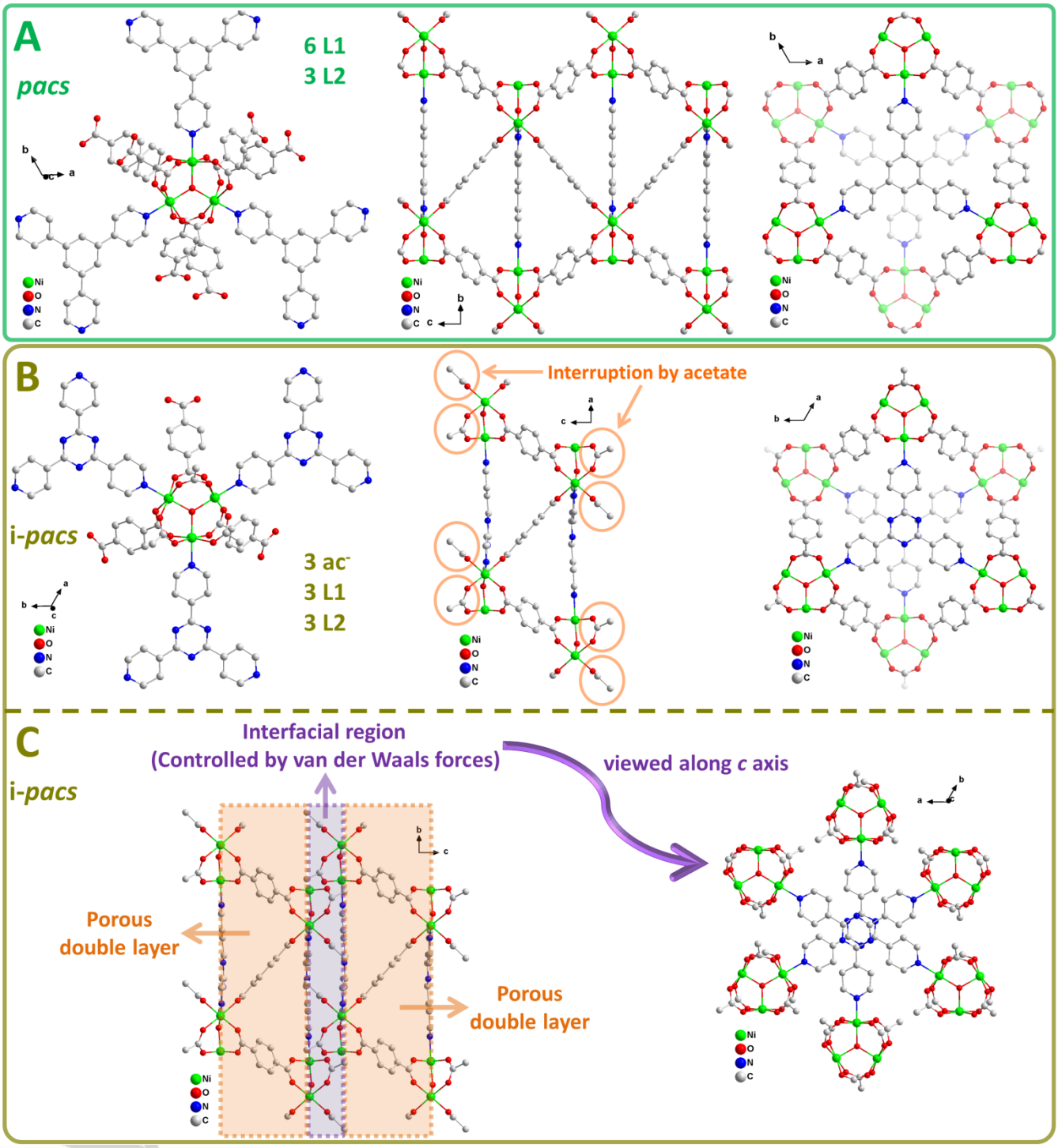

Figure 2. (A) The Ni_3 trimer and the framework structure viewed along the *a* and *c* directions for *pacs*-Ni_3-bdc-tpbz. (B) The Ni_3 trimer and one double-layer of i*pacs*-Ni_3-bdc-tpt structure viewed along different directions. (C) Two porous double-layers and their interfacial region in i*pacs*-Ni_3-bdc-tpt. The triazine rings between two tpt ligands adopt staggered cofacial stacking.

The rapid development in the synthesis of MOF materials has created scenarios where chemical interactions other than metal-crosslinker coordination interactions can be strong or pervasive enough to cause the breakdown of isoreticular chemistry and formation of other MOF structure types. One scenario is the growing interest in designing ultra-small pore MOF materials for gas separation.[3] For ultra-small pore materials, the ligand-ligand distances can be small enough so that the variation in the

backbone structures of the ligand could lead to significantly different interactions. Another scenario is the pursuit of high-connected MOF topologies which can be desirable for enhancing certain MOF properties such as stability.[4] The high-connected MOF structures can also be impacted by the size of the ligand core. The third scenario is the increasing interest in the use of bioisosteric (BIS) replacement strategy in the design of new MOF materials.[3a-c, 5] The BIS strategy is the replacement of the zero-volume benzene ring with non-aromatic cores and it often involves ligands with bulky cores (e.g., bicyclic ligands). Clearly, the use of the BIS strategy and the increased ligand-core volume can lead to much altered ligand-ligand interactions.

In this work, we choose multi-module MOF platforms to study the scope and limits of isoreticular chemistry. We focus on the *pacs* (partitioned acs) platform which is derived from the partitioning of MIL-88-type framework.[3a-d, 4b, 5h-j, 6] The *pacs* framework has the formula $[(M)_3(O/OH)(L1)_3(L2)]$ in which ditopic L1 ligand and trigonal planar M_3 trimer form acs-type framework while the pore-partitioning module (L2 ligand) divides pore space by bonding to open-metal sites of trimers. The past studies have shown that the *pacs* is a highly tolerant MOF platform and has the capacity to accommodate many M_3-L1-L2 combinations. It is thus intriguing to study factors that bring additional and tunable chemical interactions capable of challenging its tolerance level, which is useful for both optimizing the properties of *pacs* materials as well as to generate other MOF structure types with complementary properties.

Here we report a comparative study of the Ni-L1-L2-Lm system (L1: dicarboxylate, L2: tripyridyl ligand, Lm: monocarboxylate) by using four L1 ligands (bdc, bcp, cdc, bco) and three L2 ligands (tpt, tppy, tpbz) (**Figure 1**). A family of Ni-based MOF materials has been synthesized that falls into a range of structure types including Ni_3-*pacs*, Ni_3-i-*pacs*, Ni_3-muo, Ni_2-tfo, and Ni-hcb.[7] One significant finding is that there are intermediate MOF structures between two extreme situations: preservation vs. breakdown of isoreticular chemistry. One intermediate structure type is i-*pacs* (interrupted *pacs*) formed by terminating the trigonal planar $M_3(OH)$ clusters from one side of the trimer plane in *pacs*, which retains the porosity in the double layer regime (**Figure 2**). Another highlight is the establishment of a new type of isoreticular chemistry on the muo platform between two very different chemical systems: Ni_3-L1-L2-Lm (L1 = cdc, bco, L2 = tppy, tpbz) vs. Zn_4-dicarboxylate-tricarboxylate (**Figures 3 and S3.15**).[5a, 8] This type of isoreticular chemistry involving drastic changes in underlying chemistry and structural motifs has revealed new possibilities in the MOF design. The gas sorption and electrocatalytic studies were also performed that reveal excellent performance for select materials.

An important factor impacting isoreticular tolerance and its breakdown is ligand-ligand interactions. The formation of *pacs* structure is dictated by metal-ligand coordination interactions. Although the *pacs* components (e.g., L2 ligands) are capable of ligand-ligand interactions because of their large π system, such interactions yield to metal-ligand interactions and play no role in the *pacs* formation. So far, despite many efforts to compress the pacs framework, the shortest achievable distance between L2-L2 ligands in *pacs* is 4.91 Å in CoV-tcb-tpbz-act,[3c] still far larger than 3.7 Å needed for L2-L2 interactions. However, as revealed in this work, such ligand-ligand interactions are almost always on the standby and can tip the equilibrium and break the isoreticular chemistry in favor of other structure types.

By systematically studying all 12 L1-L2 combinations, we found that in the Ni-L1-L2-ac system (Hac = acetic acid), *pacs*, i-*pacs*, and Ni_3-muo are three major competing MOF structures (**Figure 4A**). We further found that among four L1 ligands, the shortest bicyclic bcp ligand shows the highest isoreticular tolerance to remain as *pacs* because all bcp-L2 (L2 = tpt, tppy, and tpbz) combinations give *pacs*. We suggest that one reason for the high isoreticular tolerance of the Ni-bcp-L2-ac system to remain as *pacs* is that the conditions for forming competing i-*pacs* or Ni_3-muo structures are not met by the bcp-L2 combination. Specifically, unlike the *pacs* type that has a wide tolerance for the L1/L2 length ratio, the muo type is complicated by two different structural roles of L2 and has a low tolerance for the variation in L1/L2 length ratio (**Figure S9.1-S9.2**). As a result, the Ni_3-muo type cannot be formed with bcp.

The i-*pacs* structure type bears the closest resemblance to pacs. To better understand the formation of i-*pacs*, the *pacs* structure can be visualized as trimer-L2 hexagonal layers pillared by slanted dicarboxylates L1 ligands. In this view, we can remove half of pillaring L1 ligands by replacing each dicarboxylate in every other layer with two acetate ligands (**Figure 2B**). This results in the partial preservation of the *pacs* structure through the formation of double layers (pillared with remaining half of L1 ligands). These acetate-decorated double layers collapse onto each other along the crystallographic *c* axis to form i-*pacs* structure. The interface between adjacent double layers is controlled by van der Waals interactions between ligands such as L2-L2, L1-acetate, and acetate-acetate (**Figure 2C**). It is worth noting that while tpt-to-tpt separation in the double layer is 7.03 Å (same as in *pacs*), suggesting no L2-L2 interactions within each double layer, the separation between two tpt molecules (L2-L2 interactions) across the interface between two double layers in Ni_3-bdc-tpt i-*pacs* is as short as 3.23 Å (**Figure 4C**), which is significantly shorter than 3.6 Å, suggesting very strong L2-L2 interactions.

To help explain why i-*pacs* cannot be synthesized with bcp, we have examined different ligand-ligand interactions. In Ni_3-bdc-tpt i-*pacs*, the shortest C-to-C distance between two acetate ligands is 3.82 Å (between one sp^3-C and one sp^2-C) which is reasonable for van der Waals interactions (**Figure 4B**). A shortening in L1 from bdc (6.85 Å) to bcp (6.01 A) would cause the corresponding shortening of the acetate-acetate distance which is not likely. This is likely a reason for the inability of bcp ligand to form i-*pacs*.

While bcp cannot form i-*pacs*, it is possible to synthesize i-*pacs* in bdc-L2 (L2 = tpt, tppy) and cdc-L2 (L2 = tpt). In Ni-bdc-L2-Hac system, bdc forms i-*pacs* with tpt, a mixture of i-*pacs* and *pacs* with tppy, and *pacs* with tpbz. This trend in favor of *pacs* over i-*pacs* going from tpt, tppy, to tpbz is likely due to the staggered L2-L2 cofacial pairing in i-*pacs* that may be more suitable for tpt (**Figure 4C**). Specifically, the staggered L2-L2 cofacial pairs allows the core aromatic ring to be closer (3.23Å in Ni_3-bdc-tpt i-*pacs*) compared to eclipsed L2-L2 cofacial paring.

The very short L2-L2 distance can cause planar L2 ligands to deviate from planarity to bowl-shaped ones, which seems the easiest for tpt (compared to tppy and tpbz). The favoring of i-*pacs* by tpt (as shown in Ni-bdc-L2) is corroborated by the Ni-cdc-L2 system where only Ni-cdc-tpt forms i-*pacs*.

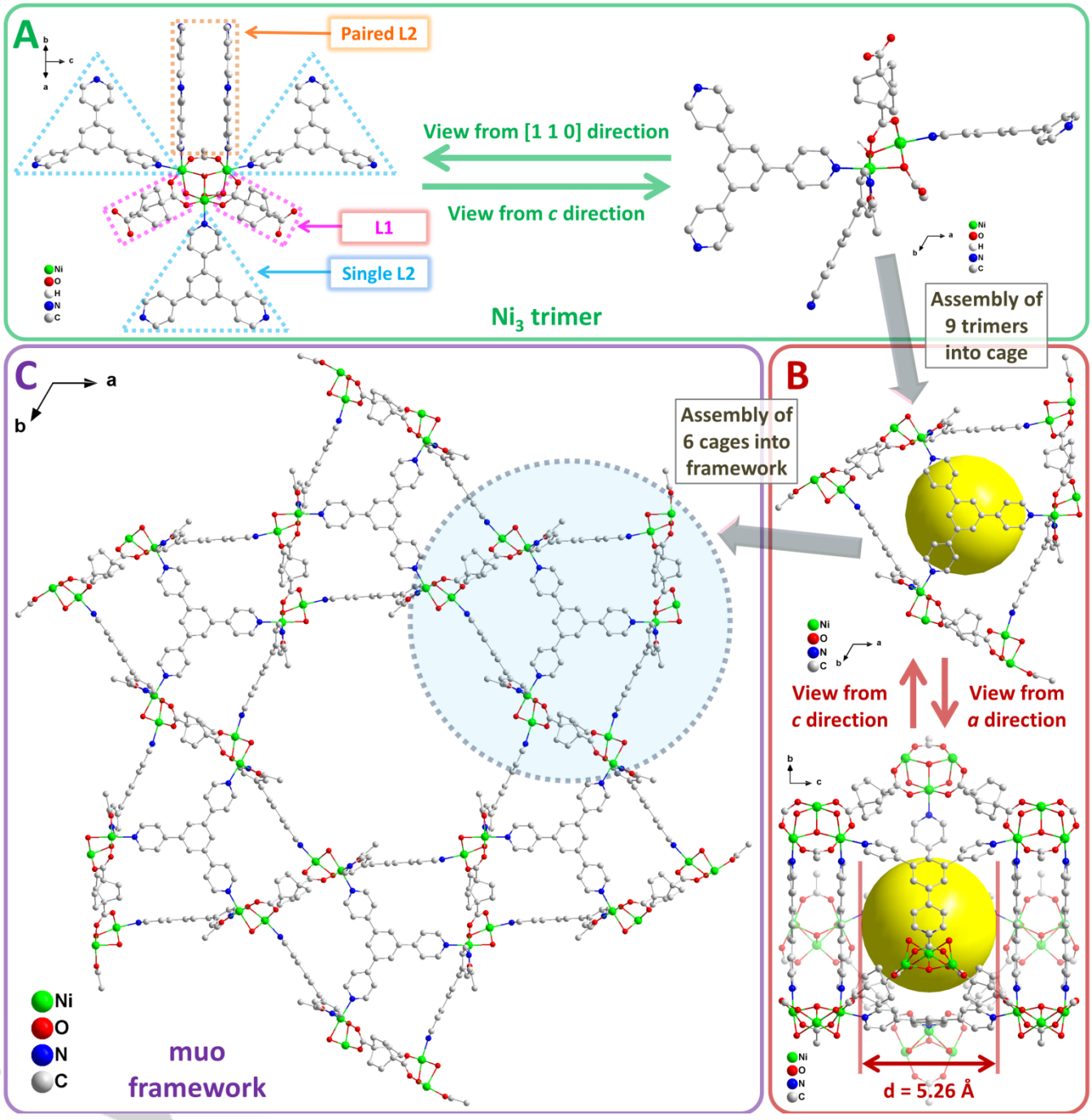

Figure 3. (A) The Ni_3 trimer of muo-Ni_3-bco-tpbz viewed along two directions. Each Ni_3 trimer connects with two L1, three single L2, and one L2 pair. The L2 pair adopts eclipsed cofacial stacking. (B) Nine trimers form a cage shown in two projections. (C) The framework viewed along the *c* direction showing a large channel.

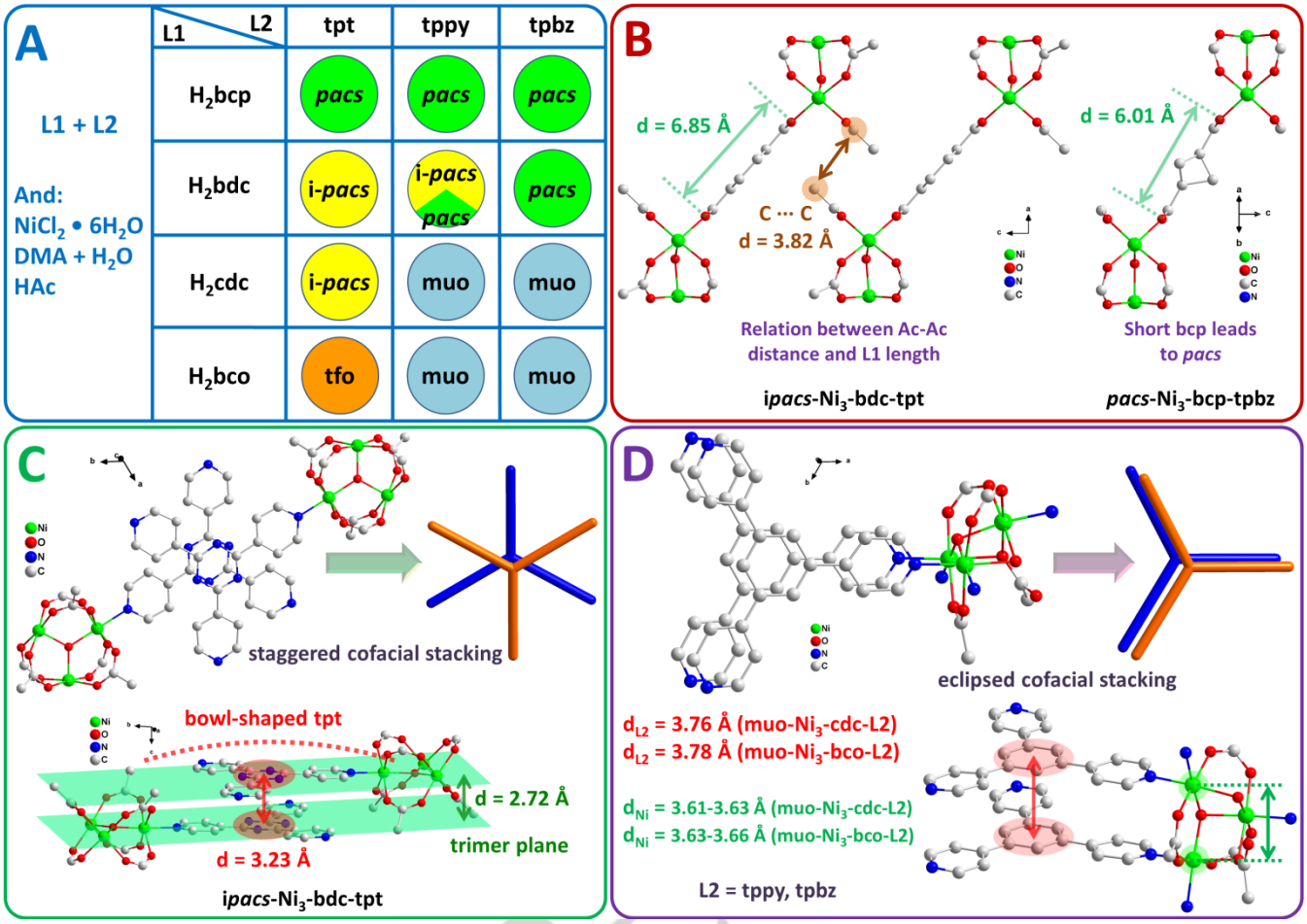

Figure 4. (A) The phase selection that is tunable with L1 and L2 types. (B) The relation between the acetate-acetate distance and L1 length in i*pacs*-Ni_3-bdc-tpt, which is a possible reason for shorter bcp not to form i-*pacs*. (C) The staggered cofacial stacking of L2 pair in i*pacs*-Ni_3-bdc-tpt favors tpt. (D) The eclipsed cofacial stacking of L2 pair in muo-Ni_3-L1-L2 structures favors tpbz.

As we move from bcp (forming *pacs*) and bdc (forming i-*pacs* or *pacs*) to more bulky bicyclic ligands (cdc and bco) in the Ni-L1-L2-Hac system, the tendency to form *pacs* or i-*pacs* is greatly diminished. With the help of tpt which favors i-*pacs*, cdc still forms i-*pacs*. However, the Ni_3-muo phase becomes an exclusive phase for cdc-L2 and bco-L2 (L2 = tppy, tpbz) composition. The formation of the eclipsed cofacial L2-L2 pair is the most critical factor for the formation of Ni_3-muo type (**Figure S3.16** and **Figure S9.4**). The (3,3,6)-connected muo topology ($P6_3/m$) was originally found in UMCM-1 in which each Zn_4O cluster is coordinated to 2 adjacent bdc linkers and 3+1 btb linkers (H_3btb = 1,3,5-tris(4-carboxyphenyl)benzene) with the formula of $[Zn_4O]_3(bdc)_3(btb)_3(btb)$. For Ni_3-muo reported here (formula: $[Ni_3(OH)_2(ac)_2]_3(L1)_3(L2)_3(L2)_2$), L1 = cdc, bco, L2 = tppy, tpbz), Zn_4O, bdc, btb, and btb in UMCM-1 are replaced with Ni_3 trimer, L1, single L2, and paired L2, respectively (**Figure 3** and **Figure S3.15**). Each Ni_3 timer connects with two L1 ligands, three single L2 ligands, and one L2-L2 pair. It is worth noting that the L2-L2 pair in Ni_3-muo adopts eclipsed cofacial stacking (**Figure 4D**).[5j, 9] There are strong experimental evidence to support that the tendency to form such eclipsed L2-L2 pairs follows the sequence tpbz > tppy > tpt. One reason that eclipsed cofacial stacking is less likely for tpt is that the eclipsed configuration between central triazine rings leads to the electronegative N atoms on top of each other. Thus, in addition to the trend observed in i-*pacs*, the synthesis of Ni_3-muo again demonstrates that the tunable ligand-ligand interactions are important parameters that can be used to control the co-assembly in multi-module MOF synthesis.

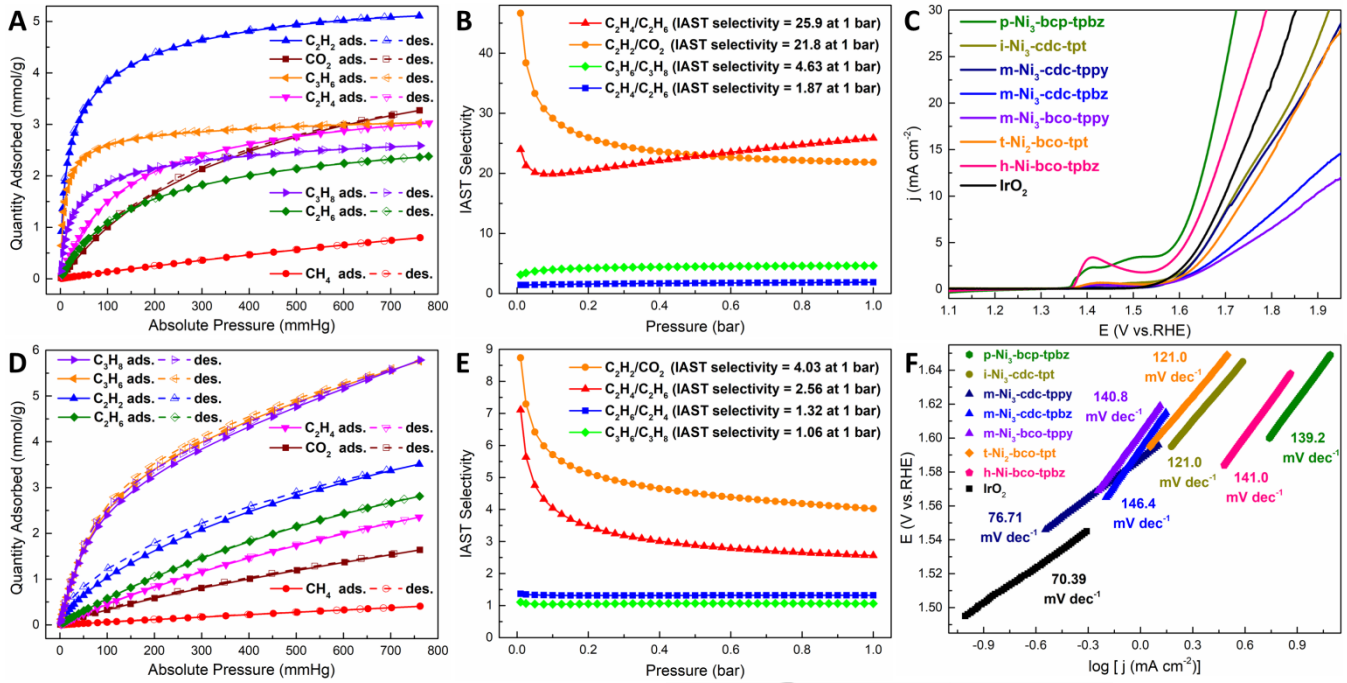

Figure 5. Gas adsorption isotherms of *pacs*-Ni_3-bcp-tpbz (A) and muo-Ni_3-cdc-tppy (D) at 298 K. IAST (50/50 v/v) selectivities for three gas pairs at 298 K of *pacs*-Ni_3-bcp-tpbz (B) and muo-Ni_3-cdc-tppy (E). For OER, the LSV curves of different catalysts (C) and the corresponding Tafel slope of different catalysts (F).

Gas sorption studies using N_2, CO_2, C_2H_2, C_2H_4, C_2H_6, C_3H_6, and C_3H_8 were performed with select materials (*pacs*-Ni_3-bcp-tpbz, i*pacs*-Ni_3-cdc-tpt, and muo-Ni_3-L1-L2). The Brunauer–Emmett–Teller (BET) surface area from N_2 sorption at 77 K (**Figure S10.1**) is 53.1 m^2/g for i*pacs*-Ni_3-cdc-tpt, 694 m^2/g for *pacs*-Ni_3-bcp-tpbz, 1289 m^2/g for muo-Ni_3-cdc-tpbz, 1310 m^2/g for muo-Ni_3-bco-tpbz, 1794 m^2/g for muo-Ni_3-bco-tppy, and 1988 m^2/g for muo-Ni_3-cdc-tppy (**Table S3.2**), indicating highly tunable porosity in *pacs* and muo structures. PXRD shows that *pacs*, i-*pacs*, muo-Ni_3-cdc-tppy, and muo-Ni_3-bco-tpbz remained stable before and after sorption (**Figure S8.1** and **Figure S8.4-S8.6**).

Both *pacs*-Ni_3-bcp-tpbz and muo-Ni_3-cdc-tppy exhibit C_2H_2/CO_2 and C_2H_2/C_2H_4 selective adsorption properties. At 298 K and 1 atm, the C_2H_2, CO_2 and C_2H_4 uptakes are 5.11, 3.27 and 3.01 mmol/g for *pacs*-Ni_3-bcp-tpbz; and 3.51, 1.64 and 2.35 mmol/g for muo-Ni_3-cdc-tppy (**Figure 5A and D**, **Table S3.2**). The isotherms of C_2H_2, CO_2, and C_2H_4 at 298 K were used to fit the Dual-Site Langmuir–Freundlich (DSLF) model to calculate the ideal adsorbed solution theory (IAST, 50/50) selectivity. For C_2H_2/CO_2, the selectivity is 21.8 for *pacs*-Ni_3-bcp-tpbz, and 4.03 for muo-Ni_3-cdc-tppy. For C_2H_2/C_2H_4, the selectivity is 25.9 for *pacs*-Ni_3-bcp-tpbz, and 2.56 for muo-Ni_3-cdc-tppy (**Figure 5B and E**, **Table S3.4**). Overall, small-pore *pacs*-Ni_3-bcp-tpbz has better C_2H_2/CO_2 and C_2H_2/C_2H_4 selective adsorption performance than muo-Ni_3-cdc-tppy with larger pores.

Ni_3-*pacs*, Ni_3-i-*pacs*, Ni_3-muo, Ni_2-tfo, and Ni-hcb synthesized here were selected for studying their performance in oxygen evolution reaction (**OER**). Among these materials, *pacs*-Ni_3-bcp-tpbz has the best electrocatalytic activity. Linear sweep voltammetry (LSV) curves of different samples are investigated (**Figure 5C**), and *pacs*-Ni_3-bcp-tpbz has relatively low overpotential of 406 mV at current density of 10 mA cm^{-2}, which is comparable to IrO_2 (**Figure S11.1B**). In contrast, the overpotential of muo-Ni_3-cdc-tppy is 495 mV at current density of 10 mA cm^{-2}. But the muo-Ni_3-cdc-tppy has relatively low Tafel slope of 76.7 mV dec^{-1}, which is comparable to IrO_2 (**Figure 5F**).

In conclusion, we have performed a systematic study of the chemical and structural factors that impact the MOF phase selection in the Ni-L1-L2-Lm system, leading to a family of Ni-MOF materials with diverse topologies. It was observed that the competitive metal-ligand interactions (M-L1, M-L2, M-Lm) and tunable ligand-ligand interactions (e.g., staggered L2-L2, eclipsed L2-L2, ac-ac) play important roles in the isoreticular tolerance and phase selection. In addition, both the length and core volume of L1 ligands have large impact, due to their effect on ligand-ligand interactions such as L1-L1 and L1-ac. The competing as well as synergistic interactions among different structural components create diverse crystallization pathways, leading to different MOF structure types with tunable gas sorption and electrochemical properties.

Supporting Information

The authors have cited additional references within the Supporting Information.[10]

Acknowledgements

We acknowledge the support of this work by the US Department of Energy, Office of Basic Energy Sciences, Materials Sciences and Engineering Division under Award No. DE-SC0010596 (P.F.). The electrocatalytic studies of the synthesized materials were supported by the National Science Foundation (CHEM 2154375, P. F.).

Keywords: isoreticular tolerance • multi-module • *pacs* • muo • metal-organic frameworks

[1] a) S. J. Lee, S. G. Telfer, *Angew. Chem. Int. Ed.* **2023**, *62*, e202306341; b) X. Li, J. Liu, K. Zhou, S. Ullah, H. Wang, J. Zou, T. Thonhauser, J. Li, *J. Am. Chem. Soc.* **2022**, *144*, 21702-21709; c) M. J. Kalmutzki, N. Hanikel, O. M. Yaghi, *Sci. Adv.* **2018**, *4*, eaat9180.

[2] a) M. Eddaoudi, J. Kim, N. Rosi, D. Vodak, J. Wachter, M. O'Keeffe, O. M. Yaghi, *Science* **2002**, *295*, 469-472; b) H. Cui, Y. Ye, T. Liu, Z. A. Alothman, O. Alduhaish, R.-B. Lin, B. Chen, *Inorg. Chem.* **2020**, *59*, 17143-17148; c) A. Dutta, Y. Pan, J.-Q. Liu, A. Kumar, *Coord. Chem. Rev.* **2021**, *445*, 214074; d) H. Jiang, D. Alezi, M. Eddaoudi, *Nat. Rev. Mater.* **2021**, *6*, 466-487; e) Z. Chen, K. O. Kirlikovali, P. Li, O. K. Farha, *Acc. Chem. Res.* **2022**, *55*, 579-591.

[3] a) H. Yang, Y. Chen, C. Dang, A. N. Hong, P. Feng, X. Bu, *J. Am. Chem. Soc.* **2022**, *144*, 20221-20226; b) Y. Xiao, Y. Chen, W. Wang, H. Yang, A. N. Hong, X. Bu, P. Feng, *J. Am. Chem. Soc.* **2023**, *145*, 10980-10986; c) W. Wang, H. Yang, Y. Chen, X. Bu, P. Feng, *J. Am. Chem. Soc.* **2023**, *145*, 17551-17556; d) Y. Chen, W. Wang, S. Alston, Y. Xiao, P. Ajayan, X. Bu, P. Feng, *Angew. Chem. Int. Ed.* **2025**, *64*, e202415576; e) K. Adil, Y. Belmabkhout, R. S. Pillai, A. Cadiau, P. M. Bhatt, A. H. Assen, G. Maurin, M. Eddaoudi, *Chem. Soc. Rev.* **2017**, *46*, 3402-3430.

[4] a) V. Guillerm, M. Eddaoudi, *Acc. Chem. Res.* **2021**, *54*, 3298-3312; b) H. Yang, F. Peng, A. N. Hong, Y. Wang, X. Bu, P. Feng, *J. Am. Chem. Soc.* **2021**, *143*, 14470-14474.

[5] a) L. K. Macreadie, R. Babarao, C. J. Setter, S. J. Lee, O. T. Qazvini, A. J. Seeber, J. Tsanaktsidis, S. G. Telfer, S. R. Batten, M. R. Hill, *Angew. Chem. Int. Ed.* **2020**, *59*, 6090-6098; b) C. S. Smoljan, R. Q. Snurr, O. K. Farha, *J. Mater. Res.* **2024**, *39*, 1047-1056; c) K. B. Idrees, K. O. Kirlikovali, C. Setter, H. Xie, H. Brand, B. Lal, F. Sha, C. S. Smoljan, X. Wang, T. Islamoglu, L. K. Macreadie, O. K. Farha, *J. Am. Chem. Soc.* **2023**, *145*, 23433-23441; d) B. Lal, K. B. Idrees, H. Xie, C. S. Smoljan, S. Shafaie, T. Islamoglu, O. K. Farha, *Angew. Chem. Int. Ed.* **2023**, *62*, e202219053; e) L. K. Macreadie, K. B. Idrees, C. S. Smoljan, O. K. Farha, *Angew. Chem. Int. Ed.* **2023**, *62*, e202304094; f) C. S. Smoljan, Z. Li, H. Xie, C. J. Setter, K. B. Idrees, F. A. Son, F. Formalik, S. Shafaie, T. Islamoglu, L. K. Macreadie, R. Q. Snurr, O. K. Farha, *J. Am. Chem. Soc.* **2023**, *145*, 6434-6441; g) C. S. Smoljan, F. Sha, P. Campitelli, H. Xie, M. A. Eddaoudi, M. R. Mian, C. Di Nicola, K. O. Kirlikovali, R. Q. Snurr, O. K. Farha, *Cryst. Growth Des.* **2024**, *24*, 3941-3948; h) Y. Xiao, A. N. Hong, Y. Chen, H. Yang, Y. Wang, X. Bu, P. Feng, *Small* **2023**, *19*, 2205119; i) Y. Chen, H. Yang, W. Wang, X. Li, Y. Wang, A. N. Hong, X. Bu, P. Feng, *Small* **2023**, *19*, 2303540; j) Y. Xiao, Y. Chen, W. Wang, X. Bu, P. Feng, *Angew. Chem. Int. Ed.* **2024**, *63*, e202403698.

[6] a) S.-T. Zheng, X. Zhao, S. Lau, A. Fuhr, P. Feng, X. Bu, *J. Am. Chem. Soc.* **2013**, *135*, 10270-10273; b) X. Zhao, X. Bu, Q.-G. Zhai, H. Tran, P. Feng, *J. Am. Chem. Soc.* **2015**, *137*, 1396-1399; c) Q.-G. Zhai, X. Bu, C. Mao, X. Zhao, L. Daemen, Y. Cheng, A. J. Ramirez-Cuesta, P. Feng, *Nat. Commun.* **2016**, *7*, 13645; d) X. Zhao, X. Bu, E. T. Nguyen, Q.-G. Zhai, C. Mao, P. Feng, *J. Am. Chem. Soc.* **2016**, *138*, 15102-15105; e) X. Zhao, C. Mao, K. T. Luong, Q. Lin, Q.-G. Zhai, P. Feng, X. Bu, *Angew. Chem. Int. Ed.* **2016**, *55*, 2768-2772; f) Y. Wang, X. Zhao, H. Yang, X. Bu, Y. Wang, X. Jia, J. Li, P. Feng, *Angew. Chem. Int. Ed.* **2019**, *58*, 6316-6320; g) Y. Wang, X. Jia, H. Yang, Y. Wang, X. Chen, A. N. Hong, J. Li, X. Bu, P. Feng, *Angew. Chem. Int. Ed.* **2020**, *59*, 19027-19030; h) H. Yang, Y. Wang, R. Krishna, X. Jia, Y. Wang, A. N. Hong, C. Dang, H. E. Castillo, X. Bu, P. Feng, *J. Am. Chem. Soc.* **2020**, *142*, 2222-2227; i) A. N. Hong, H. Yang, T. Li, Y. Wang, Y. Wang, X. Jia, A. Zhou, E. Kusumoputro, J. Li, X. Bu, P. Feng, *ACS Appl. Mater. Interfaces* **2021**, *13*, 52160-52166; j) B. Zhu, J.-W. Cao, S. Mukherjee, T. Pham, T. Zhang, T. Wang, X. Jiang, K. A. Forrest, M. J. Zaworotko, K.-J. Chen, *J. Am. Chem. Soc.* **2021**, *143*, 1485-1492; k) A. N. Hong, E. Kusumoputro, Y. Wang, H. Yang, Y. Chen, X. Bu, P. Feng, *Angew. Chem. Int. Ed.* **2022**, *61*, e202116064; l) A. N. Hong, Y. Wang, Y. Chen, H. Yang, E. Kusumoputro, X. Bu, P. Feng, *Chem. Eur. J.* **2023**, *29*, e202203547; m) Y. Xiao, Y. Chen, A. N. Hong, X. Bu, P. Feng, *Angew. Chem. Int. Ed.* **2023**, *62*, e202300721; n) W. Wang, Y. Chen, P. Feng, X. Bu, *Adv. Mater.* **2024**, *36*, 2403834; o) P. Ajayan, W. Wang, Y. Chen, X. Bu, P. Feng, *Adv. Mater.* **2024**, *36*, 2408042.

[7] Deposition Numbers 2387538 (for **m-Ni$_3$-bco-tppy**), 2387539 (for **m-Ni$_3$-bco-tpbz (condition 1)**), 2387540 (for **m-Ni$_3$-bco-tpbz (condition 2)**), 2387541 (for **m-Ni$_3$-bco-tpbz (condition 5)**), 2387542 (for **m-Ni$_3$-bco-tpbz (condition 6)**), 2387543 (for **m-Ni$_3$-cdc-tppy**), 2387545 (for **m-Ni$_3$-cdc-tpbz**), 2387546 (for **p-Ni$_3$-bcp-tpbz (condition 1)**), 2387547 (for **p-Ni$_3$-bcp-tpbz (condition 2)**), 2387548 (for **p-Ni$_3$-bdc-tppy**), 2387549 (for **p-Ni$_3$-bdc-tpbz**), 2387550 (for **i-Ni$_3$-cdc-tpt**), 2387552 (for **i-Ni$_3$-bdc-tpt**), 2387555 (for **h-Co-bco-tpbz**), 2387558 (for **h-Ni-bco-tpbz**), 2387564 (for **z-Ni-bdc-tpa**), 2387565 (for **s-Ni$_2$-bco**), 2387566 (for **t-Ni$_2$-bco-tpt (condition 1)**), 2387568 (for **t-Ni$_2$-bco-tpt (condition 3)**) contain the supplementary crystallographic data for this paper. These data are provided free of charge by the joint Cambridge Crystallographic Data Centre and Fachinformationszentrum Karlsruhe Access Structures service.

[8] a) K. Koh, A. G. Wong-Foy, A. J. Matzger, *Angew. Chem. Int. Ed.* **2008**, *47*, 677-680; b) K. Koh, A. G. Wong-Foy, A. J. Matzger, *J. Am. Chem. Soc.* **2010**, *132*, 15005-15010; c) B. Mu, P. M. Schoenecker, K. S. Walton, *J. Phys. Chem. C* **2010**, *114*, 6464-6471; d) K. K. Tanabe, C. A. Allen, S. M. Cohen, *Angew. Chem. Int. Ed.* **2010**, *49*, 9730-9733; e) M. Kim, J. A. Boissonnault, C. A. Allen, P. V. Dau, S. M. Cohen, *Dalton Trans.* **2012**, *41*, 6277-6282; f) C.-C. Liang, Z.-L. Shi, C.-T. He, J. Tan, H.-D. Zhou, H.-L. Zhou, Y. Lee, Y.-B. Zhang, *J. Am. Chem. Soc.* **2017**, *139*, 13300-13303; g) C.-S. Liu, M. Chen, J.-Y. Tian, L. Wang, M. Li, S.-M. Fang, X. Wang, L.-M. Zhou, Z.-W. Wang, M. Du, *Chem. Eur. J.* **2017**, *23*, 3885-3890; h) S. Ullah, M. A. Bustam, M. A. Assiri, A. G. Al-Sehemi, G. Gonfa, A. Mukhtar, F. A. Abdul Kareem, M. Ayoub, S. Saqib, N. B. Mellon, *Microporous Mesoporous Mater.* **2020**, *294*, 109844.

[9] a) R. Thakuria, N. K. Nath, B. K. Saha, *Cryst. Growth Des.* **2019**, *19*, 523-528; b) K. Carter-Fenk, J. M. Herbert, *Chem. Sci.* **2020**, *11*, 6758-6765.

[10] a) E. C. Constable, G. Zhang, C. E. Housecroft, J. A. Zampese, *CrystEngComm* **2011**, *13*, 6864-6870; b) O. V. Dolomanov, L. J. Bourhis, R. J. Gildea, J. A. K. Howard, H. Puschmann, *J. Appl. Crystallogr.* **2009**, *42*, 339-341; c) A. Spek, *J. Appl. Crystallogr.* **2003**, *36*, 7-13; d) W. Fan, S. Yuan, W. Wang, L. Feng, X. Liu, X. Zhang, X. Wang, Z. Kang, F. Dai,

D. Yuan, D. Sun, H.-C. Zhou, *J. Am. Chem. Soc.* **2020**, *142*, 8728-8737; e) D. Wang, B. Liu, S. Yao, T. Wang, G. Li, Q. Huo, Y. Liu, *ChemComm* **2015**, *51*, 15287-15289; f) A. L. Myers, J. M. Prausnitz, *AIChE J.* **1965**, *11*, 121-127; g) D. Hu, X. Wang, X. Chen, Y. Wang, A. N. Hong, J. Zhong, X. Bu, P. Feng, T. Wu, *J. Mater. Chem. A* **2020**, *8*, 11255-11260; h) R. D. Shannon, *Acta Crystallogr. A* **1976**, *32*, 751-767.

Entry for the Table of Contents

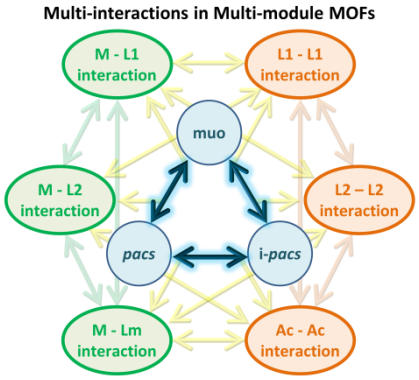

Beyond metal-ligand interactions: The scope of isoreticular chemistry is influenced by competing metal-ligand interactions (M-L1, M-L2, M-acetate) and tunable ligand-ligand interactions such as staggered L2-L2, eclipsed L2-L2, and acetate-acetate. The length and core volume of L1 ligands further impact phase outcomes through L1-L1 and L1-acetate interactions. Different balances among these forces generate diverse new MOF phases beyond the *pacs* type.